ANALYSIS OF INTERFACIAL HEAT TRANSFER COEFFICIENTS IN SQUEEZE CASTING OF AA6061 ALUMINUM ALLOY WITH H13 STEEL DIE
Impact of Section Thickness on Thermal Behavior

by

Vijay Ramarao KHAWALE[a], Ali ALSHAMRANI[b*], Satishkumar PALANISAMY[c*], Barun HALDAR[d], Sivakumar RAMAMURTHY[e], Justin Maria Hillary JOHN[f], Suresh KRISHNAMOORTHY[g], Manish SHARMA[h], and Nashmi H. ALRASHEEDI[d]

[a] Department of Mechanical Engineering,
Yeshwantrao Chavan College of Engineering, Nagpur, India
[b] Department of Mechanical Engineering, College of Engineering,
Taif University, Taif, Saudi Arabia
[c] Department of Mechanical Engineering, Rathinam Technical Campus,
Coimbatore, Tamilnadu, India
[d] Mechanical and Industrial Engineering Department, College of Engineering,
Imam Mohammad Ibn Saud Islamic University (IMSIU), Riyadh, Kingdom of Saudi Arabia
[e] Department of Physics, Easwari Engineering College (Autonomous), Tamilnadu, India
[f] Department of Mechatronics Engineering, Sri Krishna College of Engineering and Technology,
Coimbatore, Tamilnadu, India
[g] Information Technology, Sri Venkateswara College of Engineering,
Pennalur Village, Sriperumbudur, Kancheepuram, Tamilnadu, India
[h] Mechanical Engineering Department, Madanapalle Institute of Technology and Science,
Madanapalle, Andhra Pradesh, India

Original scientific paper
https://doi.org/10.2298/TSCI230310272K

A step die made of H13 steel was utilized in this investigation cast aluminum alloy AA6061 at a pressure of 95 MPa in sections measuring 3 mm, 6 mm, 9 mm, 12 mm, and 15 mm in thickness. Surface temperatures during the squeeze casting process, as well as temperatures at distances of 3 mm, 6 mm, and 9 mm from the inner wall of the die, were recorded using K-type thermocouples. Utilizing the inverse method to solve 1-D heat conduction equations, we successfully determined the interfacial heat transferring coefficients (IHTC) and the interfacial heat flux (IHF) of the cast and die surface. The calculations revealed that with the commencement of squeeze casting, there was a significant rise in the IHTC for each of the five sectional steps. These IHTC reached their peak before they began to decline. The peak range of IHTC incrementally increased with the section thickness, from the 3 mm of Step 1 up to the 15 mm of Step 5. Moreover, the rate at which the IHTC reached its peak and then stabilized at a low level was slower for steps with greater thicknesses.

Key words: *heat transfer, squeeze casting, IHTC, AA6061, casting section thickness*

[*] Corresponding authors, e-mail: a.shamrani@tu.edu.sa, sp.sathishkumar10@gmail.com

Introduction

Aluminum-silicon alloys such as AA6061 are extensively utilized in both the automotive and aerospace sectors because of their excellent balance of strength and weight, their ability to resist corrosion, and their adequate fatigue strength [1]. However, high pressure die casting, which is used in the auto parts industry, drastically affects AA6061's yield strength and ductility. The rapidity with which the molten metal is injected into the die might cause gas to become trapped within the cast material [2]. This is most apparent in pieces with a thick cross-section. For reliable casting simulations, heat transmission processes, especially at the metal/mold contact, must be well quantified.

The intricacies of heat transfer within casting cavities render the modelling of these processes challenging due to the complex transport mechanisms involved. Measurements of interfacial heat transfer coefficients (IHTC) have been recorded for various aluminum alloys [3, 4]. In the context of permanent mould casting situations, it was observed that the highest IHTC values for AA6061 alloy and A356 alloy were 3050 W/m^{2}K and 4050 W/m^{2}K, respectively. When magnesium alloy AM50 and aluminum alloy ADC12 were cast under high pressure, the IHTC increased first, fluctuated, and finally reduced significantly. During the fluctuation stage, thinner sections that were subjected to greater shot velocities demonstrated elevated IHTC values, with AM50 peaking at 12900 W/m^{2}K and ADC12 at 20760 W/m^{2}K. Furthermore, it was observed that higher initial temperatures of the die resulted in lower peak IHTC values in thicker sections [5].

Squeeze casting is a method of producing castings with superior quality, fine micro-structures, and enhanced mechanical qualities by minimising the incidence of porosity through the introduction of liquid alloy into a mould cavity without turbulent flow [6]. Squeeze casting has been studied extensively, and the results have shown that technique can create alloys with fine micro-structures and outstanding mechanical properties. Sathiaraj *et al*. [7], for instance, tried their hand at cylindrical squeeze casting with commercially pure aluminum. They took die temperatures and extrapolated to the die-metal contact using polynomial curve fitting to get an idea of what the die surface might be.

In experiments without pressure, the IHTC was found to be 2927.92 W/m^{2}K, which was in good agreement with the value of 2961.86 W/m^{2}K obtained via a numerical inverse technique [8]. At 85.86 MPa, the IHTC increased above the experimental value of 3354.12 W/m^{2}K to its maximum value of 3397.29 W/m^{2}K. In contrast, the IHTC initially reached a significantly increased value and then declined to a lower steady-state after the squeeze casting technique utilizing aluminum alloy A443 [9, 10]. When aluminum alloy A443 was compressed to 60 MPa, the peak IHTC ranged from 5631-9423 W/m^{2}K. This variation occurred across a range of casting thicknesses, which extended from 3-20 mm. However, there has been scant investigation into the nature of heat transmission during the pressured solidification of hypoeutectic AA6061 alloys of varying section thicknesses [11].

Squeeze casting with five different step thicknesses and 95 MPa of pressure was used for this experiment. The stairwell has gradations of 3 mm, 6 mm, 9 mm, 12 mm, and 15 mm. Temperature measurements were used to compute the thickness-dependent IHTC. These readings were obtained at three distinct levels: the casting surface, 6 mm below the die surface, and 9 mm below the die surface (IHTC). In this investigation, the inverse heat transfer coefficient (IHTC) was used to determine the direction and magnitude of heat transfer among the metal/die throughpressurised solidification of AA6061.

Experimental process

Materials

Tables 1 and 2 list the chemical composition and thermophysical factors of the commercially available casting aluminum alloy AA6061 used in the investigation.

Table 1. Chemical arrangement of AA6061 [wt.%]

Si	Mg	Si	Fe	Cu	Cr	Zn	Ti	Mn	Others	Al
8.5	0.8-1.2	0.4-0.8	0.7	0.15-0.4	0.04-0.35	0.25	0.15	0.15	0.15	Bal

Table 2. The AA6061 and die steel H13 thermophysical property

Alloy	Liquidus temperature, T_l [°C]	Heat capacity, C_p [J/kg K]	Solidus temperature T_s [C]	Density, ρ [kgm^{-3}]	Thermal conduction k (W/m K)
AA6061	594	964	540	2715	110
H13		462		7815	30

The second phase, an overflow, collects the contaminants from the first stream of liquid melt used to fill the hole. During the squeeze casting process, air was released from within the die through a vent situated atop the overflow. The 100 mm in diameter cylindrical sleeve at the chamber's base was where the molten metal was poured in.

The casting equipment consisted of a data collection system, an electric resistance furnace, and a hydraulic press with a capacity of 75 tone [12]. A cavity with five levels was formed by the combination of a lower die and a pair of top dies. Table 2 details the thermophysical properties of the both dies, both of which were fabricated from H13. A protective nitrogen atmosphere pervaded an electric resistance furnace during the melting process, where the temperature of the furnace was maintained at 820 °C at all times. The upper die was engineered to move along the centerline to facilitate the creation of the five distinct stages of the casting, as depicted in fig. 1. The dimensions of the lower die were 100 mm in diameter and 200 mm in height. Cartridge heaters preheated the top die to 230 °C and the bottom die to 370 °C. The metal was cast into the bottom mold at a temperature of 720 °C and subsequently squeeze cast in the top die under a pressure of 85 MPa for a duration of 30 seconds.

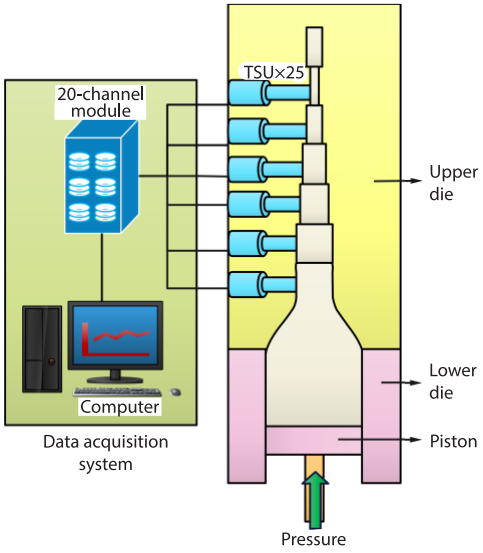

Figure 1. The process of graphically installing temperature sensor units (TSU) and the upper and lower dies in conjunction with a data collecting system

Temperature measurements

Thermocouples could be placed at precisely the right spots in each stage because to the TSU capacity for holding four of them at once. Since the TSU must undergo the same heat transfer procedure as the die, it was built out of the same H13 material [13, 14].

The *K*-type thermocouples, each with a 1.5 mm diameter, were utilized within the TSU to monitor the temperatures at which the molten metal solidifies and to gauge the temperatures at different locations of the H13 steel die five TSU pins were positioned on the right side of the die, each representing a distinct step with a wall thickness of 3 mm, 6 mm, 9 mm, 12 mm, and 15 mm. For temperature monitoring purposes, four thermocouples were assigned to each of the five steps, resulting in a total of twenty thermocouples that captured temperature data across the stages. Three thermocouples were placed 3 mm, 6 mm, and 9 mm from the inner die surface at each step to get an accurate reading of the temperature inside the die. A second thermocouple, designated *D*, was threaded through the TSU pin to take readings from the casting's outside surface. The thermocouple *D* had its head angled at 90° so that it would be firmly attached to the die. The installation method was designed to disrupt the step casting chamber's temperature field as little as possible [15, 16]. Using a data collecting system written in LabVIEW, internal chamber temperatures were continuously acquired at 500 ms intervals throughout the course of the measurement.

Inverse algorithm

Heat transfer within each step inside the die cavity was anticipated to occur by 1-D transient conduction because the thickness of the steps was much less in comparison their width or length. Because of this simplification, we could approach the issue as if it were a heat transport problem in a single dimension. We used Fourier's heat conduction equation determine the metal-to-die heat transfer coefficient [17, 18]:

$$\rho c(T)\frac{\partial T(x,t)}{\partial t}=\frac{\partial}{\partial x}\left[k(T)\frac{\partial T(x,t)}{\partial x}\right] \tag{1}$$

where d is the sensor node's (x) distance from the die surface, ρ – the die density, $c(T)$ – the specific heat capacity, T – the temperature, t – the time, and $k(T)$ – the thermal conductivity of the die change with temperature.

$$(1+2F_0)T_0^{p+1}-2F_0T_1^{p+1}=2F_0\frac{\Delta x}{k}q_0+T_0^p \tag{2}$$

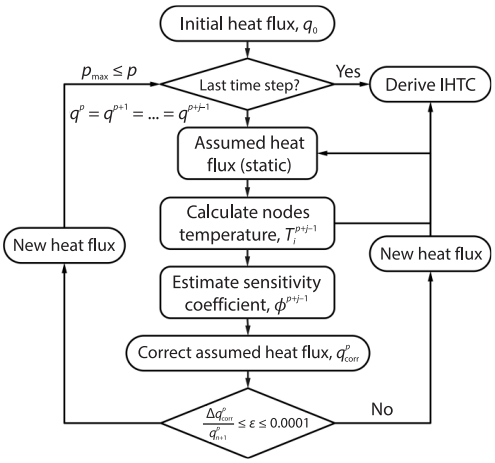

Figure 2. The IHTC estimation flowchart based on the inverse approach applied to the metal/die interface

Equation (1) can be re-written as eq. (2) for die internal sensor nodes (3):

$$(1+2F_0)T_n^{p+1}-F_0\left(T_{n-1}^{p+1}+T_{n+1}^{p+1}\right)=T_n^p \tag{3}$$

$$F_0=\frac{\alpha\Delta t}{(\Delta x)^2}=\frac{k}{c\rho}\frac{\Delta t}{(\Delta x)^2} \tag{4}$$

where p is the time step, F_0 – the Fourier frequency, α – the thermal diffusivity, c – the capacity of the heat at die, and n – the number off-grid points.

The procedure followed to calculate the IHF, q_0, at the metal and the die contact for every duration stages is shown in fig. 2 and consists of the following operations. To begin, an initial heat flux value, q_0, was presumed for the

first-time step. This value was kept constant over a set number of following time steps (where u ranges from 2-5).

By utilizing eq. (2) and the initial assumption of q_0 and the starting temperature of the die ($p = 0$), each node's predicted temperature for the next time step (3).

Next, the estimated heat flux was fine-tuned by incrementing it with a small quantity (εq_0).

The recalculated temperature distribution was obtained for the new, slightly altered heat flux ($q_0 + \varepsilon q_0$).

The process culminated with the computation of the sensitivity coefficient, ∅, through eq. (5), which is based on the partial derivative detailed in eq. (6). This procedure fundamentally utilizes the Taylor series expansion as the basis for the calculation [19]:

$$\eta^{p+j-1} = \frac{\partial T}{\partial q} = \frac{T^{p+j-1}\left[q_{n+1}^{p+j-1}\left(1+\varepsilon\right)\right] - T^{p+j-1}\left(q_{n+1}^{p+j-1}\right)}{\varepsilon q_{n+1}^{p+j-1}} \tag{5}$$

By using the boundary conditions q and $q + \varepsilon$, it is possible to solve this equation. In the numerator, temperature, Δt, represents the discrepancy in computed temperatures at the monitoring node during the similarduration step. The numerator remains unchanged at 1, however the denominator incorporates a correction for the variation in q values denoted as $\varepsilon = 0.0001$:

$$T_{n+i}^{p+j} \approx T_{n+i}^{p+j-1} + \frac{\partial T_{n+i}^{p+j-1}}{\partial q_{n+1}^{p+j}}\left(q_{n+1}^{p+j} - q_{n+1}^{p+j-1}\right) \tag{6}$$

By reducing the partial derivative of eq. (7) with respect to q to zero, we obtain eq. (6) [20]:

$$S\left(q\right) = \left(\sum_{i=1}^{I=mr}\left(T_{n+i} - Y_{n+i}\right)^2\right),\ m = \frac{\Delta\theta}{\Delta t} \tag{7}$$

$$\frac{\partial S\left(q\right)}{\partial q} = \frac{\partial}{\partial q}\left(\sum_{i=1}^{I=mr}\left(T_{n+i} - Y_{n+i}\right)^2\right) = 0 \tag{8}$$

By plugging in the solutions of eqs. (5) and (6) into eq. (8), we get:

$$\begin{gathered}\frac{\partial}{\partial q}\left(\sum_{i=1}^{I=mr}\left(T_{n+1}^{p+j-1} + \varnothing_i^{p+j-1}\left(q_{M+1}^{p+j} - q_{M+1}^{p+j-1}\right) - Y_{n+i}\right)^2\right) = 0 \\ \sum_{i+1}^{I=mr}\varnothing_i^{p+j-1}\left(T_{n+1}^{p+j-1} - Y_{n+i} + \varnothing_i^{p+j-1}\left(\nabla q_{n+1}^{p+j}\right)\right) = 0\end{gathered} \tag{9}$$

In eq. (10), we can see that the correcting term of the IHF was computed by rearrangement of eq. (9):

$$\Delta q_{n+1}^{p} = \frac{\sum_{i=1}^{l}\left(Y_{n+i} - T_{n+1}^{p+j-1}\right)\varphi_i^{p+j-1}}{\sum_{i+1}^{l=mr}\left(\varnothing_i^{p+j-1}\right)^2} \tag{10}$$

$$q_{\text{corr}}^{p} = q_{n+1}^{p} + \Delta q_{n+1}^{p} \tag{11}$$

The alterations in temperature distribution and heat flux served as the foundation for the subsequent set of computations. The aforementioned procedure was repeated indefinitely until the designated condition was fulfilled:

$$\frac{\Delta q_{n+1}^{p}}{q_{n+1}^{p}} \leq \varepsilon \tag{12}$$

After then, the IHF and the temperature of surface of the die were monitored at predetermined intervals. The following formula was used to get the heat transfer coefficient, h:

$$h = \frac{q}{T_{\mathrm{cs}} - T_{\mathrm{ds}}} \tag{13}$$

where q is the average heat transfer over the metal-die contact, h – the IHTC, T_{ds} – the temperatures of the die surface, and T_{cs} – the casting surface temperature.

The method for calculating the IHTC at the boundary between the molten alloy and the die is shown in fig. 2.

Results and discussion

Figure 3 shows how the temperature within a TSU shifts during Stage 3 when subjected to an external pressure of 85 MPa. Charts are kept of the temperatures at various depths (3 mm, 6 mm, and 9 mm below the die surface) and on the casting surface. Step 4 casting surface temperature peaked within one second of the molten alloy making contact with thermocouple *D*, as shown in the graph. The cavity was filled with the molten alloy via the bottom of the lower die, and preliminary solidification commenced due to the design of the two-piece upper die and the one-piece lower die. Even though the surface of the casting reached a high of 750 °C , that number is well below the liquidus temperature of the alloy, which was measured at 620 °C. In addition, from the bottom die's initial preheat temperature of 230 °C, temperatures at depths of 3 mm, 6 m, and 9 mm within the die grew progressively. The H13 die steel has a low thermal conductivity, hence the temperature rise at the 9 mm depth was less rapid than at the 3 mm depth.

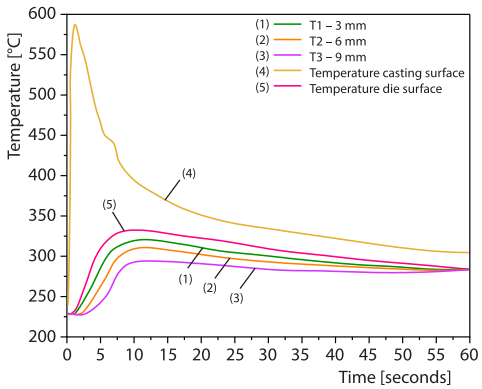

Figure 3. Evaluation of the temperature *vs.* time graphs

The TSU readings for H13 steel were taken at depths of 3 mm, 6 mm, and 9 mm in order to get an accurate picture of the temperature of the die surface. Based on the temperatures measured at the die surface and the casting surface, the IHTC and the IHF were determined after the fact, as shown in fig. 4. In the last phase, both the IHTC and heat flux peaked at 8100 W/m^{2}K and $4.51 \cdot 10^{05}$ W/m^2, respectively.

The calculated IHTC curves for all five phases are shown in fig. 5. There is a consistent trend throughout the curves, with IHTC growing rapidly at the outset. After reaching their maximum levels, IHTC began to decline. Peak IHTC values varied between 6950 W/m^{2}K and 17430 W/m^{2}K across Stages 1 through 5. Changes in IHTC over time showed that as section thickness grew, more stable connections were made between the metal and die. As a result, the peak IHTC values were strongly affected by section thickness, with greater peak IHTC values observed for sections thickness.

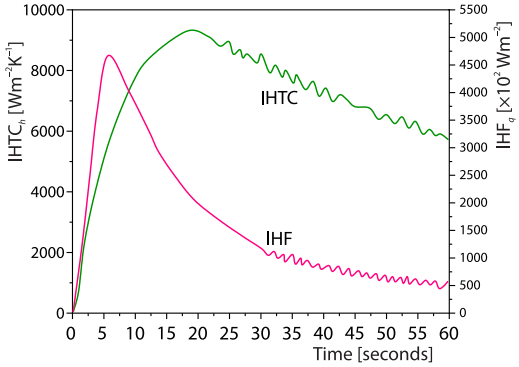

Figure 4. Utilizing the inverse approach, the IHTC, *q*, and IHF curves are computed (Step 4, 95 MPa)

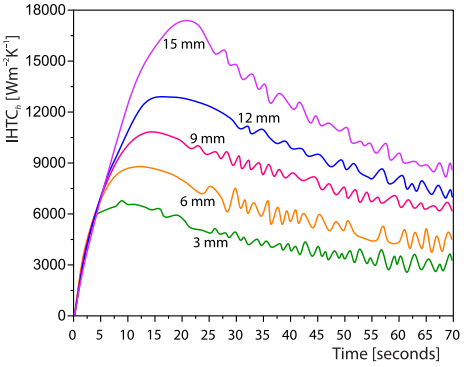

Figure 5. Time *vs.* IHTC curves for each of the five steps when 95 MPa of pressure is applied

Figure 6 depicts the time needed to attain the peak IHTC values for each of the five phases. In order to reach their peaks, the first five steps took 10.1 seconds, 12.9 seconds, 15.9 seconds, 18.7 seconds, and 21.6 seconds. Aside from variations in peak IHTC values, there was also a temporal disparity between thinner and thicker steps. Although the IHTC curves for the thicker steps fell off to lower levels quickly, reaching their maximum values took more time. As can be shown in fig. 6, the peak IHTC (5120 W/m^{2}K) and the duration required to obtain the peak IHTC (10.1-21.2 seconds) more than doubled when the section thickness was increased from 3-15 mm.

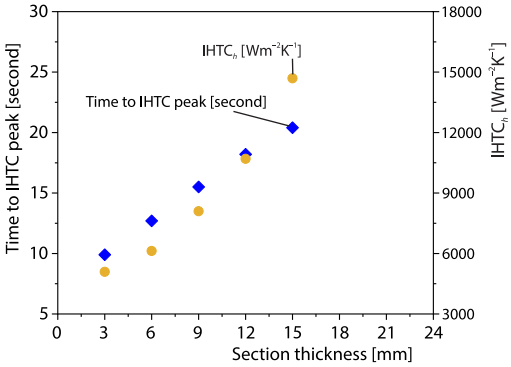

Figure 6. Peak range and lapse of time to reach IHTC peaks vary as the five-step casting's cross-section thicknesses vary

The significant impact of section thickness on IHTC values at various times is seen in fig. 5 by the time-varying IHTC curves for all five steps. Using IHTC readings recorded at 15 seconds, 30 seconds, and 45 seconds after molten alloy was poured into the die cavity, a linear relationship was established between the thickness of the casting section and IHTC. These times were chosen because they correspond to phases when IHTC levels are often at their highest.

Linear, logarithmic, exponential, polynomial, and power equations are just some of the mathematical functions used in the analysis, the results of which are presented in tab. 3. The polynomial function outperformed all other mathematical functions examined, producing the greatest correlation coefficients for the 15th, 30th, and 45th seconds, correspondingly. Figure 7 shows the results of fitting the IHTC values vs section thickness data from fig. 5 to a polynomial function over the chosen time intervals.

The regression analysis yielded empirical equations that establish a relationship between IHTC values and section thickness for the specified three-time intervals.

$$\text{In the } 1^{5th} \text{ second, } h = -15.979x^2 + 831.88x + 2906.70 \quad (14)$$

$$\text{In the } 30^{th} \text{ second, } h = -23.447x^2 + 1051.4x + 1190.10 \quad (15)$$

$$\text{In the } 45^{th} \text{ second, } h = -22.815x^2 + 935.34x + 703.53 \quad (16)$$

where x is the section thickness of the step and h represents the IHTC.

Table 3. Squeeze casting of aluminum alloy AA6061 at 95 MPa: a regression analysis

Time [second]	Maths functions	Correlation coefficient, $R2$	Empirical equations
	Logarithmic	0.9283	$h = 3871.6\ln(x) + 1146.1$
	Linear	0.9495	$h = 493.59x + 4134$
15	Logarithmic	0.9440	$h = 4346.4\ln(x) - 409.22$
	Polynomial	0.9752	$h = -14.979x^2 + 831.87x + 2906.6$
	Linear	0.9325	$h = 543.35x + 3029.5$
	Exponential	0.8918	$h = 4761.6e^{0.0573x}$
	Power	0.9717	$h = 3207.8x^{0.4755}$
30	Polynomial	0.9792	$h = -22.447x^2 + 1051{\cdot}3x + 1189.9$
	Linear	0.9158	$h = 441.67x + 2490.2$
	Exponential	0.8493	$h = 3724.6e^{0.0714x}$
	Power	0.9789	$h = 2205x^{0.6096}$
	Logarithmic	0.9568	$h = 3588.5\ln(x) - 410.50$
45	Power	0.9791	$h = 1712.2x^{0.6328}$
	Exponential	0.8183	$h = 2986.6e^{0.0728x}$
	Polynomial	0.9813	$h = -21.815x^2 + 934.33x + 702.52$

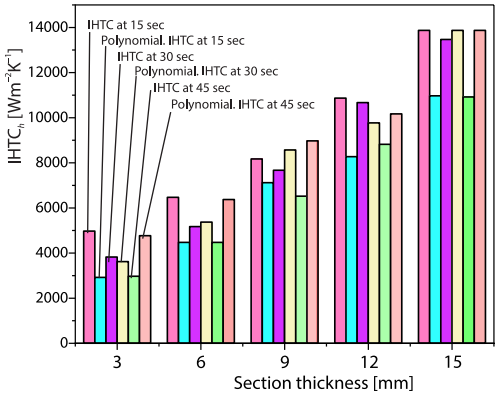

Figure 7. The regression and experimental curves depict the relationship between section thickness and interfacial heat transfer coefficients at three time points: 15 seconds, 30 seconds, 45 seconds subsequent to the filling of the die cavity with the molten alloy

Conclusions

The effective execution of squeeze casting of aluminum alloy AA6061 was achieved by adhering to a five-step technique. All of the sections that resulted had the following dimensions: 3 mm, 6 mm, 9 mm, 12 mm, and 15 mm. The 85 MPa pressure used to create them. The IHF and IHTC at interfaces were determined using the inverse approach.

Conclusions were derived from the experimental measures and computed outcomes, are as follows.

- The IHTC demonstrated a consistent pattern of change over time across distinct stages of varied thicknesses. They grew abruptly at first, peaked, and then declined steadily to their present levels. Notably, the IHTC values of thicker steps increased with increasing time.
- Squeeze casting with section thicknesses of 3 mm, 6 mm, 9 mm, 12 mm, and 15 mm yielded peak IHTC values of 5120 W/m^{2}K, 6180 W/m^{2}K, 8100 W/m^{2}K, 11700 W/m^{2}K, and 14700 W/m^{2}K when exposed to 95 MPa. Solid contact is formed between the metal and die as evidenced by an increase in peak IHTC values with increasing section thickness.
- The IHTC are significantly affected by the thickness of the casting portions. When the section thickness was extended from 3-15 mm, the maximum IHTC values increased by over

triple times, from 5120-14700 W/m^{2}K. In addition, from 10.1-20 seconds was added to the time needed to reach the peak IHTC. The thicker the step, the higher the IHTC peak value will be because of the substantial temperature fluctuations and the rigid interaction between the die and casting.

- A regression analysis of IHTC values at various times vs section thicknesses verified the viability of establishing a link between the two in step squeeze casting.

References

[1] Wang, F., *et al*., Study on the Effect of Die Coating Thickness on the Interfacial Heat Transfer Coefficient in squeeze Casting of Aluminum Alloy, *Proceedings*, 147th Annual Meeting and Exhibition Supp., Springer, New York, USA, 2018, pp. 341-347
[2] Lin, B., *et al*., Numerical and Experimental Study on Solidification Microstructure of Al-5.0Cu Alloy under Combined Fields of Power Ultrasonic and Squeeze Casting, *Jixie Gongcheng Xuebao/Journal of Mechanical Engineering*, *58* (2022), 10, pp. 87-94
[3] Zhang, X., *et al*., Interfacial heat Transfer of Squeeze Casting of Wrought Aluminum Alloy 5083 with Variation in Wall Thicknesses, *Advances in Materials and Processing Technologies*, *3* (2017), 3, pp. 407-417
[4] Venkatesh, A. P., *et al*., Experimental Study on Interfacial Heat Transfer Coefficients at the Casting/Die Interface in Squeeze Casting under Transient Condition, *International Journal of Ambient Energy*, *41* (2020), 7, pp. 802-807
[5] Wang, F., et al., Experimental study on the Heat Transfer Behavior and Contact Pressure at the Casting-Mold Interface in Squeeze Casting of Aluminum Alloy, *Int. J. Heat Mass Transf*., *112* (2017), Sept., pp. 1032-1043
[6] Sun, Z., *et al*., Section Thickness-Dependant Interfacial Heat Transfer in Squeeze Casting of Aluminum Alloy A443, In IOP Conference Series, *Materials Science and Engineering*, *27* (2011), 012073
[7] Sathiaraj, G., *et al*., The Mechanical Behavior of Nanosized Al_2O_3-Reinforced Al-Si7-Mg Alloy Fabricated by Powder Metallurgy and Forging, *ARPN Journal of Engineering and Applied Sciences*, *11* (2016), 9, pp. 6056-6061
[8] Ren, L., et al., Heat transfer at Casting/Mold Interface in Pressurized Solidification of Al Alloy A380, *Proceedings,* 5-6th Thermal and Fluids Engineering Summer Conference, ASTFE, Danbury, Conn., USA, 2021, pp. 807-816
[9] Sun, Z., *et al*., Experimental Study and Numerical Verification of Heat Transfer in Squeeze Casting of Aluminum Alloy A443, Metallurgical and Materials Transactions B, *Process Metallurgy and Materials Processing Scienc*e, *43* (2012), 6, pp. 1676-1683
[10] Li, J.-W., *et al.*, Interfacial heat Transfer Behavior of Aluminum Alloy during Squeeze Casting, *Zhongguo Youse JinshuXuebao/Chinese Journal of Non-ferrous Metals*, *24* (2014), 11, pp. 2727-2734
[11] Ramesh, B., *et al*., Optimization and Experimental Analysis of Drilling Process Parameters in Radial Drilling Machine for Glass Fiber/Nanogranite Particle Reinforced Epoxy Composites, *Mater Today Proc*., *62* (2022), Part 2, pp. 835-840
[12] Wang, F., *et al*., On the Interfacial Heat Transfer and Pressure Transmission iun Squeeze Casting: A Case Study of the Sensitivity to Materials, *Int. J. Heat Mass Transf*., *133* (2019), pp. 52-61
[13] Girimurugan, R., *et al*., Static and Total Pressure Analysis of Three Way Catalytic Convertor Using CFD, *ECS Transactions*, *107* (2022), 1, pp. 7381-7387
[14] Girimurugan, R., *et al*., Application of Deep Learning to the Prediction of Solar Irradiance through Missing Data, *International Journal of Photoenergy*, *2803* (2023), ID4717110
[15] Zhang, X., *et al*., Determination of Metal/Die Interfacial Heat Transfer Coefficients in Squeeze Casting of wrought Aluminum Alloy 7075 with variations in Section Thicknesses and Applied Pressures, *Journal Heat Transfer*, *139* (2017), 2, 022101
[16] Wang, F.-F., *et al*., Measurement of Temperature Inside Die and Estimation of Interfacial Heat Transfer Coefficient in Squeeze Casting, *China Foundry*, *14* (2017), 5, pp. 327-332
[17] Dinesh Kumar, D., *et al.*, Study of Microstructure and Wear Resistance of AA5052/B4C Nanocomposites as a Function of Volume Fraction Reinforcement to Particle Size Ratio by ANN, *Journal of Chemistry*, *2023* (2023), ID2554098
[18] Tayyab, M., *et al*., Recognition of Visual Arabic Scripting News Ticker From Broadcast Stream, *IEEE Acces*s, *10* (2022), May, pp. 59189-59204

[19] Javidikia, M., *et al*., Low and High Speed Orthogonal Cutting of aa6061-t6 under Dry and Flood-Coolant Modes: Tool Wear and Residual Stress Measurements and Predictions, *Materials*, *14* (2021), 15
[20] Omer, K., *et al*., Characterization of Heat Transfer Coefficient for Non-Isothermal Elevated Temperature Forming of Metal Alloys, *International Journal of Material Forming*, *13* (2020), 2, pp. 177-201

Paper submitted: March 10, 2023
Paper revised: September 25, 2023
Paper accepted: October 21, 2023